Beaming of High-Order Harmonics Generated from Laser-Plasma Interactions

Beaming of High-Order Harmonics Generated from Laser-Plasma Interactions

M. Yeung,[1] B. Dromey,[1] D. Adams,[1] S. Cousens,[1] R. Hörlein,[2] Y. Nomura,[2] G. D. Tsakiris,[2] and M. Zepf[1,3,*]

[1]Department of Physics and Astronomy, Queen's University Belfast, BT7 1NN Belfast, United Kingdom
[2]Max-Planck-Institut für Quantenoptik, Hans-Kopfermann-Straße 1, D-85748 Garching, Germany
[3]Helmholtz-Institut Jena, Fröbelstieg 3, 07743 Jena, Germany

(Received 25 July 2012; published 18 April 2013)

Beam divergences of high-order extreme ultraviolet harmonics from intense laser interactions with steep plasma density gradients are studied through experiment and Fourier analysis of the harmonic spatial phase. We show that while emission due to the relativistically oscillating mirror mechanism can be explained by ponderomotive surface denting, in agreement with previous results, the divergence of the emission due to the coherent wake emission mechanism requires a combination of the dent phase and an intrinsic emission phase. The temporal dependence of the divergences for both mechanisms is highlighted while it is also shown that the coherent wake emission divergence can be small in circumstances where the phase terms compensate each other.

DOI: 10.1103/PhysRevLett.110.165002 PACS numbers: 52.59.Ye, 42.65.Ky, 52.35.Mw, 52.38.−r

The generation of high-order harmonics from intense laser interactions provides a unique route to extreme ultraviolet (XUV) light pulses with attosecond (10^{-18} s) duration [1]. Such pulses have a myriad of potential applications for both the measurement and the control of ultrashort subfemtosecond phenomena, particularly the atomic scale dynamics of electron wave packets [2].

High harmonic generation (HHG) from solid density plasma surfaces [3] has the potential to generate XUV pulses with extreme peak brightness. Currently, the two main understood mechanisms are the relativistically oscillating mirror (ROM) model and coherent wake emission (CWE). If the normalized laser vector potential ($a_0^2 = I\lambda^2/1.38\times10^{18}\,\mathrm{W\,cm^{-2}}\,\mu\mathrm{m}^2$, where I is the laser intensity and λ is the laser wavelength) is greater than unity, the plasma surface oscillates at relativistic velocities and can introduce a large Doppler up-shift to the reflected light resulting in ROM harmonics [4]. The CWE mechanism [5] is associated with Brunel absorption [6] whereby electrons are pulled out from the plasma density gradient (formed during the rising edge of the laser pulse) by the laser electric field component normal to the surface. Upon reversal of the sign of the electric field, these electrons are driven back into the plasma and form a high density bunch with attosecond duration. These bunches displace the electrons in the density gradient as they pass, causing them to oscillate at their local plasma frequency. These plasma oscillations can linearly couple into electromagnetic modes in a process that is the inverse of resonance absorption [7]. This mechanism is efficient for conditions where Brunel absorption dominates, namely, steep density gradients and intensities $\gtrsim 10^{16}$ W cm^{-2}.

Application of these sources requires detailed understanding and control of experimental parameters that influence the beam divergence. Previous work has shown that curvature of the plasma surface due to denting caused by the radiation pressure of the laser pulse dominates the divergence behavior of the ROM harmonics [8–10]. Effectively, the ROM harmonics are generated over a concave surface which focuses the beam to some point in front of the target. CWE harmonics can be efficiently generated over a much wider range of intensities and thus can be a more attractive prospect for subplasma frequency harmonics; however, the divergence characteristics and, in particular, its temporal evolution are not well understood.

At subrelativistic intensities ($a_0 < 1$), the divergence of CWE generated harmonics is known to be heavily influenced by the strongly intensity dependent intrinsic phase associated with the trajectories of the Brunel electrons which are responsible for driving the CWE emission [11,12]. Over a typical Gaussian or Airy profile focus, the variation of intensity across the spot leads to the emission of harmonics with curved wave fronts, and because larger intensities lead to shorter emission delays, the wave-front curves outward in the middle, much like the effect of a diverging lens. In fact, it was shown that this could be somewhat precompensated by moving the target into the focusing beam so that the curved wave fronts of the driving laser partially cancel out the intrinsic phase induced curvature [11]. This intrinsic phase effect can be very strong and is generally the reason attributed to the larger beam divergence typically seen for CWE harmonics [8,13,14].

An experiment to characterize harmonic beam divergences for both mechanisms at relativistic intensities ($a_0 > 1$) was carried out at the Rutherford Appleton Laboratory using the titanium sapphire ASTRA laser. After improving the pulse contrast at $<$500 fs before the pulse peak to $>10^9$:1 by the use of a plasma mirror [15], the laser delivered 400 mJ in a 50 fs pulse. Using an $f/3$ off-axis parabola focusing optic, a peak intensity of $\approx 2\times10^{19}$ W cm^{-2} in a near-diffraction limited spot was obtained. The target, sub-nm surface roughness fused silica

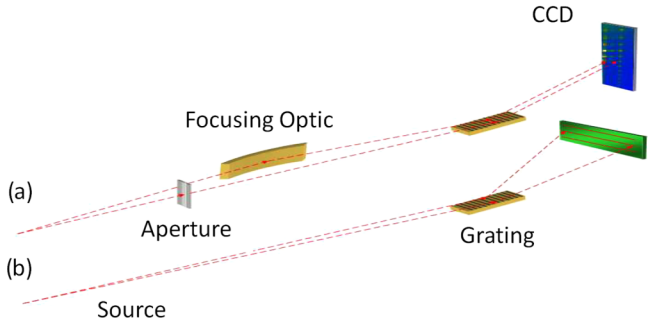

FIG. 1 (color online). Spectrometer configurations. (a) Separation of harmonic signal into on- and off-axis components. On-axis emission apertured to a 0.25 mrad cone while off-axis emission at angles between 35 and 50 mrad was collected onto the CCD using a gold focusing mirror. (b) No apertures or focusing optics to obtain the pure spectrally resolved angular distribution while the CCD was rotated so as to observe a larger cone angle.

slabs, was placed at an angle of incidence of $\approx 30°$ and a Hitachi flat field spectrometer collected the specular beam. The spectrometer was used in two configurations, as shown in Fig. 1. Spectrometer configuration 1(a) was used to characterize the angular divergence of CWE and ROM harmonics on a single shot basis, simultaneously distinguishing between on and off specular axis emission. The mirror collected harmonic radiation emitted into angles of approximately 35–50 mrad, focusing it onto the ≈ 20 CCD pixels or 0.75 mrad/pixel. This gives the appearance of a much stronger signal off axis compared to direct illumination with each pixel subtending only 0.023 mrad/pixel. Configuration 1(b) was used to allow direct measurements of the beam divergence. The experimental setup on ASTRA is also described in detail in previous publications [8,16].

Results from configuration 1(a) for two different focal positions are shown in Fig. 2. The recorded off-axis emission has a clear cutoff at the 19th harmonic which corresponds to the expected maximum plasma frequency from

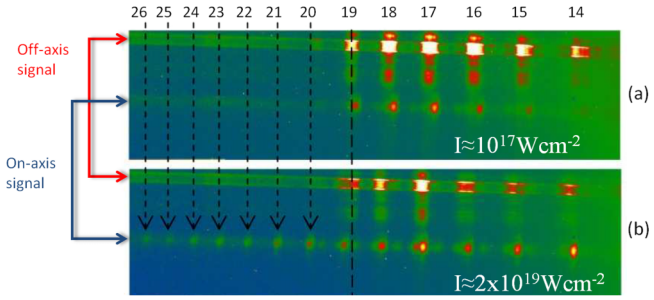

FIG. 2 (color online). Transition from the lower intensity ($\approx 10^{17}$ W cm^{-2}) CWE mechanism to the relativistic ROM ($\approx 2 \times 10^{19}$ W cm^{-2}) using the setup in Fig. 1(a). Target placed (a) 200 μm from best focus and (b) at best focus. The CWE cutoff harmonic (19th) is indicated by the extended dashed black line.

fully ionized fused silica. This observation, combined with their existence even at defocused subrelativistic intensities, distinguishes these orders as predominantly CWE. Indeed, the ROM harmonics seen beyond the CWE cutoff only appear at the highest intensity (best focus), indicating that this is clearly the transition intensity regime [17]. The two mechanisms also exhibit very distinct divergence characteristics. Measurements taken using spectrometer configuration 1(b) are compared directly in Fig. 4(b). As has been noted previously [8], the divergence of the ROM harmonics is significantly below those of the CWE harmonics under identical irradiation conditions.

The ROM divergence behavior is well understood; as mentioned previously, it is due to the denting of the target surface. However, the CWE orders exhibit divergences that, although larger than for the ROM, are much closer to the diffraction limit than previously reported measurements at much lower intensities [18]. The explanation is quite straightforward: the surface dent imposes a phase front curvature (converging) on the harmonic beam as it is emitted which directly opposes that of the intrinsic phase due to the intensity dependent bunch return times (diverging). At the higher intensities studied here, the dent becomes comparable to the intrinsic phase and the balancing of these terms leads to an overall flatter wave front. To quantitatively investigate this effect we attempt to model the harmonic divergence, focusing on harmonics 19 (CWE) and 20 (ROM) to best illustrate the distinct behaviors of the two generation mechanisms for very similar wavelengths.

To model the beam properties one must first consider the transverse spatial coherence of the harmonic source. Stochastic effects in the generation mechanism can destroy the phase correlation across the harmonic source. For example, Zhang *et al.* [19] suggested that, for picosecond duration pulses, Rayleigh-Taylor-like instabilities can ripple the target surface and destroy the transverse coherence resulting in very wide angular emission. For the ultrashort pulses described here, such instabilities do not have sufficient time to grow. Mulser *et al.* showed that Brunel electrons that return to the plasma after two laser periods have chaotic return velocities [20]. Fortunately, the electron trajectories that lead to the formation of the high density bunches that drive the CWE process are those that return in less than one period and whose return velocities have a well-defined relationship with the emission phase (which is, in fact, what allows the bunching to occur). Furthermore, it has been experimentally verified that harmonic emission from multiple sources of CWE is highly coherent [21], which can indicate good spatial coherence of an individual source, although this was not explicitly analyzed. Although it is yet to be experimentally confirmed, it is expected that ROM harmonics will share this property.

Given that we have a spatially coherent harmonic source, the divergence then depends only on the intensity distribution (principally the source size) for a given

harmonic order w_q and the spatial phase variation across the source. In our model we consider two main contributions to the spatial phase for ROM and CWE—a geometrical (''denting'') phase originating from the dynamical variation of the surface shape due to ponderomotive denting [10,22] and any intensity dependent phase terms intrinsic to the production process itself. The intrinsic phase of ROM harmonics scales as $\xi \sim 2.7a_0/n$ (where n is the normalized plasma density) and is a small [8,23] effect in the limit of high densities and moderate a_0. Consequently, the ROM phase is dominated by surface denting for our parameters. For the CWE orders we consider the dent phase and the intrinsic phase due to the intensity dependent bunch return times [11,12].

In our model the individual phase terms were calculated in a semianalytical model for each optical cycle and the spatiotemporal evolution of the harmonic phases was used to calculate the time-dependent far-field distributions for ROM and CWE. We assume that there is no coupling between these phase terms, which can be shown to be valid only because the motion of the Brunel electrons is relativistic when they reenter the plasma for our intensities. At lower intensities this assumption fails; however, the divergence becomes almost entirely dominated by the CWE intrinsic phase.

The CWE intrinsic phase effect was calculated using the numerical model that is described in more detail in Ref. [12]. In this model, the CWE mechanism follows a three-step process similar to one used to describe HHG in gaseous media [24]. The trajectories of the Brunel electrons were calculated from the relativistic equation of motion:

$$\frac{d\beta}{dt} = a_0\omega \sin\theta(1+\sqrt{1-f})(1-\beta^2)^{3/2} \times [\cos(\omega t + \omega t_0 + \phi) - \cos(\omega t_0 + \phi)], \quad (1)$$

and the intrinsic phase was taken to be the delay between the laser phase and the time at which the bunch of Brunel electrons reaches a distance of $\lambda/10$ beyond the critical surface. In this equation, $\beta = v/c$ where the electron velocity is v, ω is the laser angular frequency, θ is the angle of incidence, f is the fractional absorption, t is the time after the electron ejection time t_0, and ϕ is the carrier-envelope phase. For this analysis we approximate f to be zero or that absorption of the laser at the critical surface is negligible. We have also confirmed that changing the crossing point from $\lambda/10$ to shorter distances to account for surface denting does not significantly affect the phase variation as a check of our assumption that the intrinsic and dent phase can be considered independently.

We have also self-consistently considered the influence of the generated high harmonic fields on the returning bunches. Relatively high assumed efficiencies for the harmonics ($\approx 1\%$) were required to noticeably alter the bunch return times, but in this case a small adjustment in the intensity that was well within experimental error was able to reproduce results from runs without the inclusion of the harmonic fields; hence, we do not consider their effect important for this particular study. We note that the generated attosecond pulse fields have been shown to be able to sweep electrons away from the plasma surface where they are subsequently able to interact with, and be accelerated by, the specularly emitted fields over many laser cycles [25].

Meanwhile, the temporal evolution of the geometrical surface dent due to the laser pressure was deduced from particle-in-cell (PIC) simulations using the 1D code PICWIG [26]. The average plasma surface position was extracted for each cycle of the pulse while simulations were performed for a range of peak intensities. Each peak intensity value was mapped onto the modeled focal spot intensity distribution and the surface position, from the corresponding PIC simulation, was used to determine the phase at each cycle to be used in the model. The other simulation parameters were a peak density of $400n_c$ (n_c is the critical density), a 100 nm linear density ramp, a 30 fs FWHM Gaussian pulse shape, and mobile ions.

To model the divergence accurately, the source size must also be known. The intensity dependence of the harmonic signal is required as this determines the ratio of the harmonic source size w_q relative to the laser spot w_0 and also the relative contribution of the temporally dependent divergence to the final beam distribution. CWE is known to be approximately a linear process across a broad range of intensities [5] (however, it is sensitive to plasma gradient conditions which are also strongly tied to the pulse intensity [27]), whereas the ROM mechanism is expected to be linear only in the ultrarelativistic regime ($a_0 \gg 1$) where, for harmonics below a certain rollover order, the efficiency is predicted to depend only on the harmonic order [28]. The intensity regime considered here covers the transition to relativistic intensities where the ROM harmonic efficiency is highly nonlinear ($I_n \propto I^x$ where previous results have found $x \approx 4.0 \pm 0.5$ [8,29] or $x \approx 5.0 \pm 2.3$ [30]).

The laser spot is modeled as an idealized Gaussian with a FWHM of 2.5 μm while the temporal profile is modeled as a 30 fs FWHM Gaussian and the intensity is 2×10^{19} W cm^{-2}. As the CWE mechanism is a linear process, the source size is assumed to match that of the laser. Taking the nonlinearity of the ROM mechanism as I^4 leads to a ROM source with a FWHM that is half that for the laser in space and time. Using this model for spatiotemporal phase and harmonic source intensity, a 1D Fourier transform of the spatial distribution at each cycle was used to generate the time-dependent angular distribution for the 19th (CWE) and 20th (ROM) harmonics as shown in Figs. 3(a) and 3(b). The $1/e^2$ radius for the ROM order shows a continuous increase until the latter stages of the laser pulse as the depth of the dent increases under the pressure of the laser. Interestingly, the effect of the dent is reduced at the end tail of the pulse where the PIC simulations show that the plasma surface ''pushes back'' towards the ion front in agreement

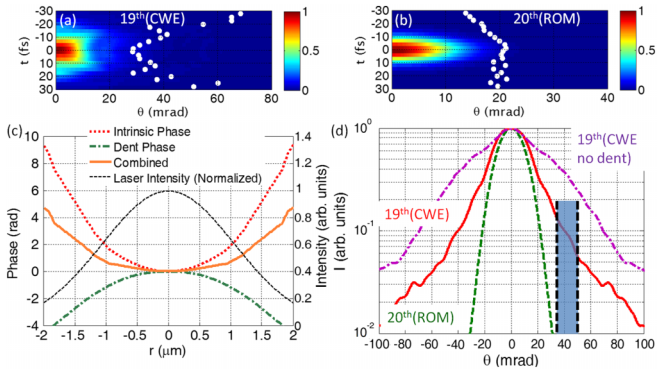

FIG. 3 (color online). Fourier analysis of the different divergence behavior for CWE and ROM for a Gaussian laser focus with a FWHM of 2.5 μm, a pulse duration of 30 fs, and a peak intensity of 2×10^{19} W cm^{-2}. Normalized angular distributions for each laser cycle for the 19th harmonic (CWE) (a), with both the intrinsic and dent phase, and for the 20th harmonic (ROM) (b), with only the dent phase considered. The white dots indicate the $1/e^2$ beam radius at each laser cycle. (c) Balancing of phase terms at where the beam radius is a minimum for the 19th harmonic. The normalized laser intensity is also shown. (d) Temporally summed angular distributions for the 19th harmonic (solid curve) and the 20th harmonic (dashed curve). Also shown is the 19th harmonic with the dent phase excluded (dot-dashed curve). The shaded region corresponds to that collected in the experiment as the off-axis emission.

with the study by Behmke *et al.* [31] where this effect was studied with regard to the temporal structure of the upshifted light. Here we observe that in the higher intensity cases this effect is stronger so that the overall effect across the spot is to flatten the harmonic phase in the latter stages of the pulse. The CWE order follows a slightly more complex behavior where the defocusing effect of the intrinsic phase dominates in the early stages of the pulse followed by a decrease in beam radius as the dent phase grows. The contribution of the various phase terms for the 19th harmonic for the cycle where the CWE divergence is minimum is plotted in Fig. 3(c). The combined phase is largely flat over the FWHM leading to the smaller divergence for that cycle.

The time integrated distribution for these parameters is given in Fig. 3(d). Not only does the CWE order have a larger beam radius, but the more complicated phase structure also leads to a significant fraction of the signal distributed into the far wings of the pulses. As shown by the shaded area, the off-axis region collected by our spectrometer is completely dominated by the CWE order in good agreement with the experimental results shown in Fig. 2. Comparing the case where the dent phase is not included in the model reveals a much larger beam divergence.

As has previously been pointed out, ROM divergence can be effectively controlled by using top-hat beam profiles or shaped targets [9], and both ROM and CWE divergence can be influenced by using the wave-front curvature out of best focus to compensate [11]. Additionally, the opposite sign and comparable magnitude of the two CWE phase terms should allow the CWE divergence to be optimized in tight focus. The intensity dependence of the time integrated divergence of the 19th order is shown in Fig. 4(a) for all other conditions as previously described. As the dent grows it is able to better compensate the intrinsic phase; thus, the general trend is for the divergence to decrease down to a minimum around 1.7×10^{20} W cm^{-2}, where, it should be noted, the ROM efficiency will start to dominate as we move into strongly relativistic intensities. In Fig. 4(b) the calculated divergences for different intensities are also compared with experimental data (shaded region). The model matches the experimental data remarkably well considering the simplicity of the model strongly suggests that it has captured the main contributions to the harmonic beam divergence in this intensity regime. It is worth noting that the temporally changing divergence will also affect the temporal profile in the far field. In particular, for CWE collecting a diffraction limited angular window will also lead to significant temporal gating of the emission for intensities close to the optimum shown in Fig. 4(a).

Note that in our experiment we calculate the diffraction limited divergence for CWE to be of the order of 10 mrad or q times less than the laser divergence θ_0 and that our experimental results (40 mrad) are much *lower* than previous claims of diffraction limited CWE emission [18]. This apparent disagreement can be explained by the fact that in the previous paper [18] the CWE emission was incorrectly assumed to be a perturbative process ($I_q \propto I_0^q$ for the qth order). Applying this assumption leads to a harmonic source size which decreases with harmonic order ($w_q \propto w_0^{\sqrt{q}}$ for Gaussian sources) and hence a predicted divergence of $\theta_q \propto q^{-1/2}$. Applying the current knowledge

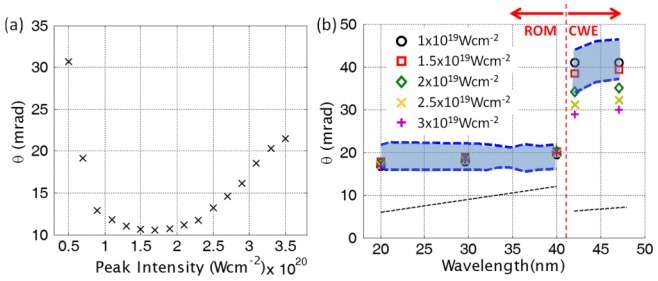

FIG. 4 (color online). (a) Divergence for the 19th harmonic calculated from the model for different intensities. Divergence values determined from Gaussian fits. At low intensities the intrinsic phase dominates, but as the intensity increases the denting phase can compensate and produce a narrower beam. At very high intensities the surface dent begins to dominate. (b) The $1/e^2$ beam radii obtained from Fourier analysis for (from the right) harmonics 17, 19, 20, 27, and 40 at different peak intensities. Laser parameters are the same as for Fig. 3. The black dotted line shows the divergence for flat phase (diffraction limited) for the modeled Gaussian sources. The dashed blue lines indicate the upper and lower error bounds for the experimentally measured harmonic divergence (as previously reported in [8]).

of the field it can be seen for the reported parameters ($a_0 < 1$ and harmonics below the CWE cutoff) that the observed harmonic signal was due to CWE, which is known to be a linear process and thus experiences no reduction of the source size. Our analysis suggests that the previous measurements were not indicative of a diffraction limited beam but instead consistent with a low intensity interaction where the CWE intrinsic phase leads to substantial defocus and the denting contribution is comparatively small.

In conclusion, experimental measurements for high-order harmonic beam divergences for intensities in the relativistic transition regime have been reported. Our results demonstrate that the divergence of harmonic sources from overdense plasma surfaces has dynamically varying beam divergence which will also affect the temporal structure in the far field. The ROM divergence is less complex since it is dominated by the denting term while the divergence of CWE harmonics depends on the subtle interplay of intrinsic and denting phase allowing for control of the CWE divergence. The modeled spatiotemporal phase behavior of the harmonics was found to match the data well and this improved understanding should allow better control of the beam properties of this unique XUV source.

*m.zepf@qub.ac.uk

[1] G. Sansone, L. Poletto, and M. Nisoli, Nat. Photonics **5**, 655 (2011).
[2] F. Krausz and M. Ivanov, Rev. Mod. Phys. **81**, 163 (2009).
[3] C. Thaury *et al.*, Nat. Phys. **3**, 424 (2007).
[4] R. Lichters, J. Meyer-ter-Vehn, and A. Pukhov, Phys. Plasmas **3**, 3425 (1996).
[5] F. Quéré, C. Thaury, P. Monot, S. Dobosz, Ph. Martin, J.-P. Geindre, and P. Audebert, Phys. Rev. Lett. **96**, 125004 (2006).
[6] F. Brunel, Phys. Rev. Lett. **59**, 52 (1987).
[7] D. E. Hinkel-Lipsker, B. D. Fried, and G. J. Morales, Phys. Fluids B **4**, 559 (1992).
[8] B. Dromey *et al.*, Nat. Phys. **5**, 146 (2009).
[9] R. Hörlein, S. G. Rykovanov, B. Dromey, Y. Nomura, D. Adams, M. Geissler, M. Zepf, F. Krausz, and G. D. Tsakiris, Eur. Phys. J. D **55**, 475 (2009).
[10] S. C. Wilks, W. L. Kruer, M. Tabak, and A. B. Langdon, Phys. Rev. Lett. **69**, 1383 (1992).
[11] F. Quéré, C. Thaury, J.-P. Geindre, G. Bonnaud, P. Monot, and Ph. Martin, Phys. Rev. Lett. **100**, 095004 (2008).
[12] P. Heissler *et al.*, Appl. Phys. B **101**, 511 (2010).
[13] F. Quéré, C. Thaury, H. George, J. P. Geindre, E. Lefebvre, G. Bonnaud, S. Hüller, P. Monot, and Ph. Martin, J. Mod. Opt. **55**, 2711 (2008).
[14] C. Thaury, F. Quéré, H. George, J. P. Geindre, P. Monot, and Ph. Martin, Eur. Phys. J. Special Topics **175**, 43 (2009).
[15] B. Dromey, S. Kar, M. Zepf, and P. Foster, Rev. Sci. Instrum. **75**, 645 (2004).
[16] R. Hörlein *et al.*, New J. Phys. **10**, 083002 (2008).
[17] A. Tarasevitch, K. Lobov, C. Wünsche, and D. von der Linde, Phys. Rev. Lett. **98**, 103902 (2007).
[18] A. Tarasevitch, A. Orisch, D. von der Linde, Ph. Balcou, G. Rey, J.-P. Chambaret, U. Teubner, D. Klöpfel, and W. Theobald, Phys. Rev. A **62**, 023816 (2000).
[19] J. Zhang *et al.*, Phys. Rev. A **54**, 1597 (1996).
[20] P. Mulser, S. M. Weng, and T. Liseykina, Phys. Plasmas **19**, 043301 (2012).
[21] C. Thaury, H. George, F. Quéré, R. Loch, J.-P. Geindre, P. Monot, and Ph. Martin, Nat. Phys. **4**, 631 (2008).
[22] M. Zepf *et al.*, Phys. Plasmas **3**, 3242 (1996).
[23] D. an der Brügge and A. Pukhov, Phys. Plasmas **14**, 093104 (2007).
[24] P. B. Corkum, Phys. Rev. Lett. **71**, 1994 (1993).
[25] J. P. Geindre, R. S. Marjoribanks, and P. Audebert, Phys. Rev. Lett. **104**, 135001 (2010).
[26] S. G. Rykovanov, M. Geissler, J. Meyer-ter-Vehn, and G. D. Tsakiris, New J. Phys. **10**, 025025 (2008).
[27] B. Dromey *et al.*, Phys. Rev. Lett. **102**, 225002 (2009).
[28] T. Baeva, S. Gordienko, and A. Pukhov, Phys. Rev. E **74**, 046404 (2006).
[29] P. A. Norreys *et al.*, Phys. Rev. Lett. **76**, 1832 (1996).
[30] P. Heissler *et al.*, Phys. Rev. Lett. **108**, 235003 (2012).
[31] M. Behmke *et al.*, Phys. Rev. Lett. **106**, 185002 (2011).